8-1-2020

The apoptotic effect of GSK-3 inhibitors: BIO and CHIR 98014 on H1975 lung cancer cells through ROS generation and mitochondrial dysfunction.

Theodore Lemuel Mathuram
Nova Southeastern University

Thiagarajan Venkatesan
Nova Southeastern University

Jayanta Das
Nova Southeastern University

Umamaheswari Natarajan
Nova Southeastern University, un15@nova.edu

Appu Rathinavelu
Nova Southeastern University, appu@nova.edu

Biotechnol Lett (2020) 42:1351–1368
https://doi.org/10.1007/s10529-020-02861-w

ORIGINAL RESEARCH PAPER

The apoptotic effect of GSK-3 inhibitors: BIO and CHIR 98014 on H1975 lung cancer cells through ROS generation and mitochondrial dysfunction

Theodore Lemuel Mathuram · Thiagarajan Venkatesan · Jayanta Das · Umamaheswari Natarajan · Appu Rathinavelu

Received: 17 January 2020 / Accepted: 6 March 2020 / Published online: 31 March 2020

Abstract
Objective GSK-3 has been reported to be upregulated in malignant diseases, including lung cancers, thus suggesting it to be a valid target for cancer treatment. The study elucidates the possible mechanism involved in the ability of GSK-3 inhibitors: BIO and CHIR 98014 to regulate proteins involved in cell death of H1975 lung cancer cells.
Results BIO and CHIR 98014 successfully induced apoptosis at lower concentrations in H1975 cells but not in H460 lung cancer cells. Moreover, increased ROS generation and depolarization of mitochondrial membrane potential were observed in both treatments. Cleavage of caspase-3 was observed in both BIO and CHIR 98014-treated cells after 72 h with monolayer and tumorsphere cell culture models.
Conclusions The use of GSK-3 inhibitors shows promising apoptotic abilities in clinical cancer treatments, particularly for lung cancer cells. This study is the first report to describe the significant apoptotic effects of BIO and CHIR 98014 through multiple mechanisms of H1975 NSCLC that are linked to their proliferative and migratory capacities.

Keywords GSK-3 inhibitors · Cancer · BIO · CHIR 98014 · Lung cancer · H1975 · H460

T. L. Mathuram · T. Venkatesan · J. Das · U. Natarajan · A. Rathinavelu (✉)
Rumbaugh-Goodwin Institute for Cancer Research, Nova Southeastern University, Ft. Lauderdale, FL 33314, USA
e-mail: appu@nova.edu

A. Rathinavelu
Health Professions Division, College of Pharmacy, Nova Southeastern University, Ft. Lauderdale, FL 33314, USA

Introduction

NSCLC (Non-small cell lung cancer) is the most common type of lung cancer, accounting for 84% of all lung cancer diagnoses made in the United States of America (Siegel et al. 2020). Among various mutations that are known to cause lung cancers, KRAS is considered to be an essential gene that is linked to aggressive growth and poor prognosis (Adderley et al. 2019). A recent report has suggested that overexpression of GSK-3 can also be indicative of poor prognosis, and therefore, its inhibition could reduce cell proliferation in lung cancers (Kazi et al. 2018). GSK-3 (Glycogen Synthase Kinase-3) is a serine/threonine kinase known to be participating in the regulation of β-catenin signaling (Wnt signaling). Glycogen Synthase kinase regulates the establishment of a multi-component destruction complex that initiates the phosphorylation of β-catenin, leading to the inactivation of Wnt signaling. The role of GSK-3β in regulating β-catenin signaling and degradation has been reported in many forms of human cancer (Walz

et al. 2017). Therefore, GSK-3 inhibitors such as BIO and CHIR have been reported to produce anti-cancer effects by inducing apoptosis in melanoma, ovarian, and pancreatic cancer cells (Yu and Zhao 2016). While GSK-3 inhibitors are maintaining diverse usage in regenerative medicine, diabetes, and CNS disorders, their usage in cancer is re-emerging in the form of combination therapies. Interestingly, GSK-3 inhibitors, in combination with anti-LAG-3 antibody, was shown to inhibit the metastasis of melanoma in humans (Rudd et al. 2020). Similarly, GSK-3 inhibitor-9-ING-41 was found to have increased efficacy in combinations with other anti-cancer drugs in various cancer types (Anraku et al. 2020). The study presented here is the first of its kind to show the efficacy of GSK-3 inhibitors, BIO and CHIR 98014 as apoptotic inducers in H1975 non-small cell lung cancer (NSCLC) cells. The primary aim of this study was to assess the role of ROS (Reactive Oxygen Species) in disturbing the mitochondrial membrane potential ($\Delta\psi_m$) and triggering apoptosis through the cleavage of caspases. In addition, the study also aimed to investigate the concentration-dependent inhibitory effects of BIO and CHIR 98014 on colony formation and the migratory abilities of H1975 cells. In summary, with tangible evidence, we have elucidated the possible mechanism through which BIO and CHIR 98014 induce apoptosis and ROS generation in H1975 cells, thus facilitating insights into targeted therapies for NSCLC.

Methods

Materials

GSK-3 inhibitors- BIO (2′Z,3′E)-6-Bromoindirubin-3-oxime, dimethylsulfoxide (DMSO) were purchased from Sigma Aldrich (MO, USA) and CHIR 98014 was purchased from Selleckchem (TX, USA). Phosphate buffered saline (PBS) with Ca^{2+} and Mg^{2+}, 1X Trypsin–EDTA solution (0.25%), 2,7- dichlorofluorescein diacetate (DCFDA, for ROS detection), CellEvent™ Caspase-3/7 Green ReadyProbe™, Bicinchoninic acid (BCA) protein assay, B-27™ (50X) supplement were purchased from Thermo Fisher (CA, USA). JC-1 dye (mitochondrial membrane potential) was purchased from Abcam (MA, USA). Bovine serum albumin (BSA) was purchased from VWR Life sciences (PA, USA). Thiazolyl Blue tetrazolium bromide (MTT) was purchased from Alfa Aesar (MA, USA). 100X Antibiotic Antimycotic Solution (with penicillin, streptomycin, and amphotericin B) was purchased from (Corning Life Sciences (MA, USA). RIPA (Radio-Immunoprecipitation Assay) buffer, protease inhibitor cocktail, and sodium orthovanadate were purchased from Santa Cruz Inc. (TX, USA) Unconjugated primary antibodies against total GSK-3, phospho-GSK-3 (Ser9), phospho-P53, XIAP, BAX, caspase-3, P21, caspase-9, LC3B, β-Catenin Antibody Sampler Kit were purchased from Cell Signaling Technology (MA, USA). Antibodies against β-actin and HRP conjugated secondary antibodies were purchased from Sigma Aldrich (MO, USA). The nitrocellulose membranes (0.45 µm) used for western blotting were purchased from GE Healthcare Life Sciences (MA, USA), and the ECL reagent was purchased from KPL BioSolutions (MA, USA).

Cell culture

The H1975, H460 and HUVEC cells were obtained from the American Type Culture Collection (VA, USA). The H1975 cells are NSCLC type with KRAS wildtype (*wt)* gene and H460 cells are large cell lung cancer type with KRAS mutant (*mt)* gene. The H460 cells are relatively aggressive in their growth ability because of KRAS mutation and therefore are widely used for various studies related to lung cancer metastasis and drug resistance. Both H1975 and H460 cells were maintained in a humidified atmosphere at 37 °C with 5% CO_2, supplemented with RPMI-1640, 1% Antibiotic/Antimycotic solution, 10% FBS obtained from Atlanta Biologicals (GA, USA). The HUVEC cells are derived from the endothelial veins of umbilical cord and represent a suitable model to study the cytotoxic effects of drugs to endothelium (Cao et al. 2017). This cell model can be used to accurately mimic transendothelial migration of cancer cells in an in vitro system (Arefi et al. 2020). The HUVEC cells were cultured with EGM™-2 Endothelial growth medium supplemented with growth factors from Lonza Inc. (NJ, USA). All experiments were conducted with 85% to 90% confluency of cells and used from after 3 passages for stabilization of cells in culture and discarded after a maximum of 13 passages.

MTT assay

MTT (3-(4,5-dimethylthiazol-2-yl)-2,5-diphenyl tetrazolium bromide) is a salt that is converted by metabolically active cells to insoluble purple-blue formazan crystals, which corresponds to the total number of live cells. Experiments were performed as three replicates in 96-well culture plates, purchased from VWR Life sciences (PA, USA). Briefly, 1×10^4 cells/well were seeded in flat-bottomed 96-well culture plates under standard culture conditions. Both H460 and H1975 cells were allowed to attach overnight and treated with BIO, CHIR 98014 using concentrations ranging from 1 and 15 μM for 24, 48, and 72 h. Following drug treatments, MTT dissolved in PBS at 5 mg/mL was added and incubated at 37°C for an additional 45 min and then the formazan crystals were dissolved using 200 μL of DMSO. The color obtained from the solubilized formazan was measured at 560 nm in a VersaMax ELISA Microplate Reader (Molecular Devices Inc., CA, USA). All experiments were done in triplicates.

BrdU (5-bromo-2′-deoxyuridine) assay

The cell proliferation of H1975 cells was assessed by measuring the incorporation of BrdU into cellular DNA using the kit that was purchased from Cell Signaling Technology (MA, USA) (Wojtowicz and Kee 2006). Briefly, H1975 cells were treated with BIO, CHIR 98014 at concentrations of 0.5, 1, and 10 μM for 72 h. Following 24 h of drug treatment, BrdU was added, and the cells were allowed to incubate till 48 h. Finally, after 72 h of drug treatment, the cells were incubated with HRP-linked anti-mouse IgG antibody to recognize the bound BrdU antibody, which was further developed by the HRP substrate TMB (3,3′,5,5′-Tetramethylbenzidine). Cell proliferation was indicated by an increased intensity of color that was directly proportional to the quantity of BrdU incorporated into cells. The absorbance was measured at 450 nm in a VersaMax ELISA Microplate Reader (Molecular Devices Inc., CA, USA). All experiments were done in triplicates.

DCFDA staining

Briefly, H1975 cells were treated with BIO, CHIR 98014 at concentrations of 0.5, 1, and 10 μM for 72 h. Following drug treatments, the cells were washed and incubated with 10 μM (DCFDA) for 10 min. DCFH-DA is a cell-permeable dye that can be deacetylated by cellular esterases to a non-fluorescent compound, which is later oxidized by ROS into 2′,7′-dichlorofluorescein (DCF). The oxidized DCF is a highly fluorescent compound that can be quantified with excitation/emission at 495 nm/529 nm (Kalyanaraman et al. 2012). During the assay, the excess dye was removed with 1X PBS washes, and cells were observed at 10X magnification using a Leica microscope (DMI3000B). The fluorescence was further quantified by spectrofluorimetry analysis with excitation/emission at 495 nm/529 nm in a 96-well plate format using Victor^2 1420 Multilabel Counter (Perkin Elmer, MA, USA). All experiments were done in triplicates.

JC-1 staining

Mitochondrial membrane potential ($\Delta\psi_m$) is considered to be a valuable indicator for metabolically active cells and has been measured using the JC-1, a lipophilic cyanine dye, capable of entering the mitochondria and forming reversible red fluorescent J aggregates in healthy cells. Contrastingly, in unhealthy cells, J aggregates are not formed due to increased membrane permeability, thus emitting green fluorescence (Perelman et al. 2012). During our experiments, the H1975 cells were treated with BIO, CHIR 98014 at concentrations of 0.5, 1, and 10 μM for 72 h. After drug treatments, the cells were washed with 1X dilution buffer and incubated with 10 μM of JC-1 for 30 min at 37 °C. Excess dye was removed using necessary washes with 1X PBS and then the fluorescence images were captured at 10X magnification under a Leica microscope (DMI3000 B) using a 10-ms exposure time in both the "green" and "red" emission channels for the fluorescence of monomers emitted at 527 nm and the aggregates at 590 nm. All experiments were done in triplicates.

Cell event^{TM} caspase-3/7 detection probe

Caspase-3 activation is an essential event in the induction of apoptosis leading to loss of cell viability. CellEvent^{TM} Caspase-3/7 probe is designed to bind to the DNA and emit a bright fluorescence when the DEVD peptide is cleaved from the conjugate, in

response to caspase-3/7 activation. Briefly, H1975 cells were treated with 0.5, 1, and 10 μM of BIO, CHIR 98014 for 72 h. Following treatment, cells were incubated with 5 μM of cell event caspase-3/7 probe for 30 min at room temperature. Cells were analyzed under a Leica microscope (DMI3000 B) at 10X magnification, using a 10-ms exposure time with apoptotic cells emitting green fluorescence at excitation 503 nm and emission 530 nm. Spectrofluorimetry analysis was further performed to quantify the fluorescence with excitation/emission at 503 nm/530 nm in a 96-well plate format using Victor^2 1420 Multilabel Counter (Perkin Elmer, MA, USA). All experiments were done in triplicates.

Tumorsphere formation assay—Cell Event™ caspase-3/7 detection probe

Cells growing in 3D cultures have been regarded with an increasing degree of importance due to greater biological relevance to the tissues or tumors growing under the in vivo conditions. Essentially, cells in colonosphere culture tend to form aggregates through the secretion of ECM, which fabricates an environment that is closer to the tumor microenvironment (TME) of the whole body (Genovese et al. 2020). The assay was performed to establish the ability of H1975 to form tumorspheres in the presence and absence of BIO for a duration of 72 h. During this assay, the H1975 cells supplemented with B27™ were cultured on ultra-low attachment plates along with BIO, CHIR 98014 at concentrations of 0.5, 1, and 10 μM for 72 h. Following treatment, cells were incubated with 5 μM of CellEvent ™ Caspase-3/7 Green Detection probe for 30 min at room temperature. After incubation, the cells were analyzed at 10X magnification under a Leica microscope (DMI3000 B) using a "green" emission channel with 10-ms exposure time and excitation/emission at 503 nm / 530 nm. To spectrofluorimetrically quantify the fluorescence, the tumorspheres were incubated with 5 μM of CellEvent ™ Caspase-3/7 Green Detection probe for 30 min at room temperature, and the readings were obtained in a 96-well plate format using Victor^2 1420 Multilabel Counter (Perkin Elmer, MA, USA). All experiments were done in triplicates.

Trans-well endothelial cell migratory assay (Boyden chamber assay)

Trans-well endothelial migration assay was performed to assess the migratory potential of H1975 cells when treated with GSK-3 inhibitors: BIO and CHIR 98014 for 72 h on a monolayer HUVEC culture. Briefly, HUVEC cells were seeded on the upper chamber of the trans-well inserts in a 24-well format with 8 μm pore size. After 24 h, H1975 cells were introduced to the upper chamber of the insert along with GSK-3 inhibitors: BIO and CHIR 98014 at concentrations 0.5, 1, and 10 μM for 72 h. Migratory H1975 cells were able to pass through the HUVEC-seeded polycarbonate membrane and attach to the bottom side while non-migratory cells remained in the upper chamber. After the drug treatments, a cotton-tipped applicator was used to carefully remove cells from the top of the membrane. Migrated H1975 cells towards the underside of the trans-well membrane were stained with MTT, which was a slight modification to a previously published method by Muller WA et al. (Muller and Luscinskas 2008). The MTT stained cells were imaged at 10X magnification under a Leica microscope (DMI3000 B). Additionally, the viability of the migrated H1975 cells stained with MTT was quantified by solubilizing formazan crystals and measuring the absorbance at 560 nm in a VersaMax ELISA Microplate Reader (Molecular Devices Inc., CA, USA). The cell viability was calculated by using the following equation: Cell viability (%) = (Absorbance of sample/Absorbance of control) × 100. All experiments were done in triplicates.

Clonogenic (cfu) assay

Clonogenic assay was performed to assess the ability of H1975 cells to form colonies under the influence of GSK-3 inhibitors: BIO and CHIR 98014 (Mathuram et al. 2017). Briefly, 4×10^3 cells were seeded onto 60 mm Tissue Culture-treated dish (Corning Life Sciences (MA, USA) overnight and incubated with BIO, CHIR 98014 at concentrations of 0.5, 1, and 10 μM for 3 weeks. Following 3 weeks of treatment, MTT, which stains the metabolically viable cells, was added and incubated for 30 min. Images were captured with a Nikon DSLR camera, H1975 colonies were manually counted and graphed with PRISM V7.

Western blotting

The H1975 cells treated with 0.5, 1, and 10 μM of BIO, CHIR 98014, were lysed with RIPA buffer containing the protease inhibitor cocktail. Supernatants were collected by centrifugation at 10,000 rpm for 30 min at 4 °C. The protein concentrations were determined using the bicinchoninic acid (BCA) protein assay method, according to the manufacturer's protocol. After normalization of protein concentrations, 30 μg of protein samples were subjected to electrophoresis using 7.5%, 10%, 12% SDS-PAGE, and blotted onto nitrocellulose membranes. The transferred membranes were probed for (GSK-3, phospho-GSK-3, phospho-P53, P21, XIAP, BAX, LC3B, caspase-3, and caspase-9). The protein bands were visualized using the LumiGLO Reserve Chemiluminescent substrate, and the luminescent images were captured using the LI-COR Odyssey Fc Imaging System (2800) and ImageJ was used to perform densitometric analysis.

Statistical analysis

Data was presented with error bars representing mean ± S.D and values representing $*P < 0.05$, $**P < 0.01$ were considered as statistically significant with one-way analysis of variance (ANOVA) and Bonferroni analysis.

Results

BIO and CHIR 98014 reduces cell viability/proliferation in H1975 cells

BIO and CHIR 98014 were experimentally observed for their ability to reduce cell viability in H1975 and H460 cells. The dose response curve generated using the cell viability data revealed 85% ± 3.3 and 75% ± 3.5 cell viability, respectively, after 24 and 48 h of treatment with 3 μM concentration of BIO. Similarly, 75% ± 4.2 and cell viability was observed with CHIR 98014 (3 μM) for 24 and 48 h of treatment. However, 1 μM concentration of BIO showed only 78% ± 8.5 reduction in cell viability after 72 h (Fig. 1a) of treatment. Whereas a higher reduction in cell viability (65% ± 5.7 ($**P < 0.01$) was observed after 72 h of treatment with CHIR 98014 (1 μM) concentration (Fig. 1b). Interestingly, H460 cells showed no significant reduction in cell viability after 24, 48, and 72 h of treatment with lower concentrations (1–10 μM). However, a statistically significant reduction in cell viability of H460 was observed at concentrations beyond 10 μM with BIO or CHIR (Fig. 1c, d). While measurable cell death responses were observed after GSK-3 inhibition, it appears that cell cycle arrest reflected by reduction in cell proliferation appears to be preceding the cell death events following the inhibition of GSK-3 by BIO or CHIR. Treatment of BIO (0.5 μM) and CHIR 98014 (0.5 μM) demonstrated 83.17% ± 3.4 and 53.9% ± 2.2 ($**P < 0.01$) reduction in cell proliferation, respectively (Fig. 1e, f). A further decrease in cell proliferation was observed, 48.4% ± 1.8 ($**P < 0.01$) and 34.4% ± 2.5 ($**P < 0.01$) respectively in BIO (1 μM) and CHIR 98014 (1 μM) treatments. However, after treatment of cells with 10 μM concentrations of BIO and CHIR 98014 the percentage of cell proliferation were greatly reduced to 24.1% ± 3.21 ($**P < 0.01$) and 18.7% ± 2.11 ($**P < 0.01$), respectively.

BIO and CHIR 98014 induces ROS in H1975 cells

The possibilities of ROS production mediating the apoptosis signals following BIO and CHIR 98014 treatments in H1975 cells were explored (Fig. 2). Increased ROS generation was observed when cells treated with 1 and 10 μM of BIO (Fig. 2c, d) as well as CHIR 98014 (Fig. 2g, h). Spectrofluorimetric quantification of DCHF-DA staining exhibited 14.6% ± 5.0 increase in fluorescence due to oxidation by ROS generated by BIO (0.5 μM) treatment for 72 h while CHIR 98014 (0.5 μM) exhibited no significant increase in the fluorescence for 72 h compared to untreated controls (Fig. 2i). However, a marginal increase in fluorescence intensity was observed with BIO (1 μM) after 72 h of treatment, while CHIR 98014 (1 μM) exhibited 64.1% ± 17.4 increase in fluorescence was observed due to ROS mediated oxidation of the probe. As anticipated (10 μM) concentration of BIO and CHIR 98014 demonstrated the highest ROS generation at (69.1% ± 10.4 and 83.9% ± 8.2) ($**P < 0.01$), respectively.

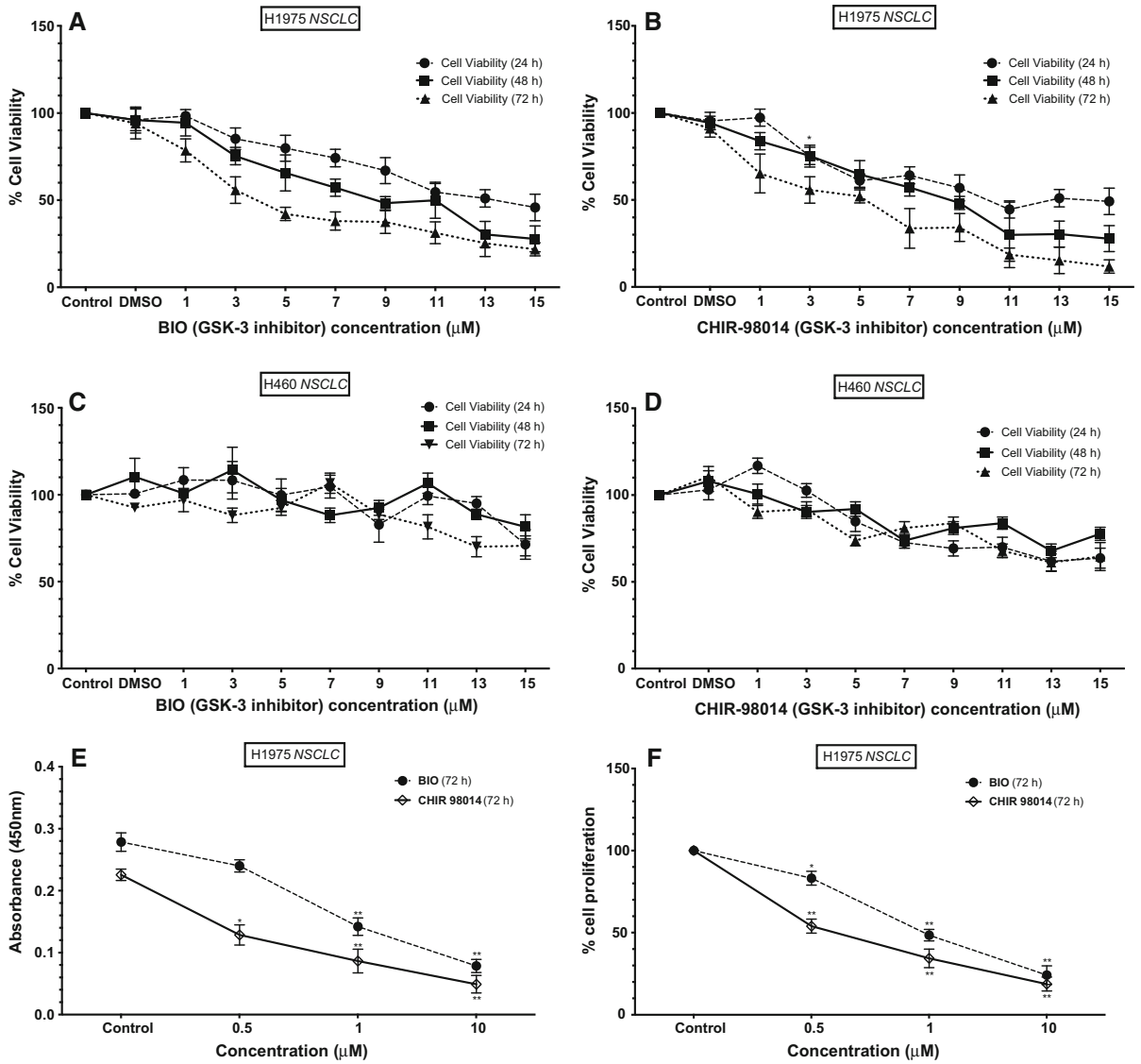

Fig. 1 MTT assay for BIO (**a**, **c**) treated H1975 cells (1—15 μM for 24, 48, 72 h), CHIR 98014 (**b**, **d**) treated H1975 cells (1—15 μM for 24, 48, 72 h). A significant reduction in cell viability was observed after treatment with 1 μM of CHIR 98014 and BIO for 72 h. **e** BrdU assay of 10 μM BIO and CHIR 98014-treated H1975 cells demonstrated significant reduction (**P < 0.01) in cell proliferation. All experiments were done in triplicates

BIO and CHIR 98014 induces mitochondrial membrane potential damage in H1975 cells

JC-1 staining confirmed the mitochondrial damage caused by BIO and CHIR 98014 treatments in H1975 cells (Fig. 3). Control cells exhibited bright red fluorescence with low green fluorescence indicating that the mitochondria membrane potential was normal, whereas 10 μM BIO-treated cells emitted more green fluorescence with low red fluorescence indicating a decrease in the mitochondria membrane potential (Fig. 3d). Thus, due to alteration in the mitochondria membrane potential, the red fluorescence was changing to green in H1975 cells treated with 0.5, 1, and 10 μM BIO and CHIR 98014 (Fig. 3d, h).

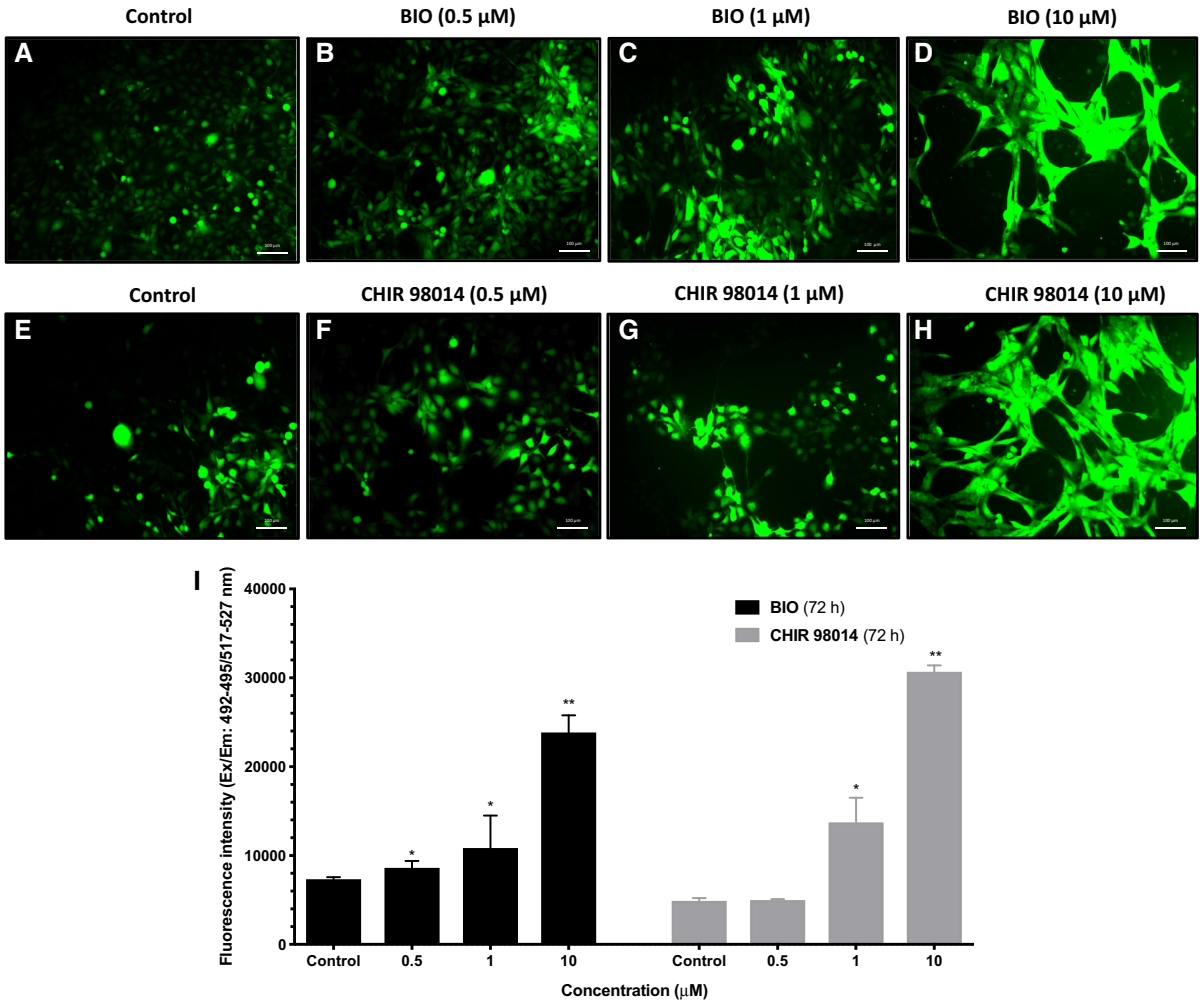

Fig. 2 Reactive Oxygen Species (ROS) detection in 0.5, 1, and 10 µM of BIO (**a–d**) CHIR 98014 (**e–h**) treated H1975 cells by DCHF-DA staining. **i** Spectrofluorimetric quantification of 10 µM BIO and CHIR 98014 for 72 h exhibited green fluorescence indicative of ROS generation due to the conversion of DCFDA to DCF accompanied by enlarged phenotypic changes. Images were taken at 10X magnification. All experiments were done in triplicates

BIO and CHIR 98014 induces activation of Caspase-3/7 in H1975 cells

Both BIO and CHIR 98014 were able to activate caspase-3/7 by proteolytic cleavage of the DEVD conjugated dye in H1975 cells that were measured using a fluorescent microscope (Fig. 4). The Cell Event™ staining showed increased fluorescence indicative of caspase-3 mediated cleavage after treating the cells with 10 µM of BIO and CHIR 98014 (Fig. 4d, h). Spectrofluorimetric quantification of fluorescence following treatment of cells with 0.5 µM BIO for 72 h exhibited no changes compared to controls (Fig. 4i) while treatment with 0.5 µM of CHIR 98014 exhibited 53.2 ± 2.6 increase in fluorescence indicating activation of caspase-3/7. Also, treatment with 1.0 µM of BIO and CHIR 98014 exhibited 15.5% ± 3.5 and 57.0% ± 8.2 increases respectively in fluorescence intensity and 10 µM BIO exhibited 32.8% ± 4.1 increase while CHIR 98014 (10 µM) exhibited 77.0% ± 2.2 (**$P < 0.01$) increase in fluorescence intensity compared to untreated controls after 72 h treatments, suggesting stronger activation of caspase-3/7 at higher concentrations which was further confirmed by western blotting analysis.

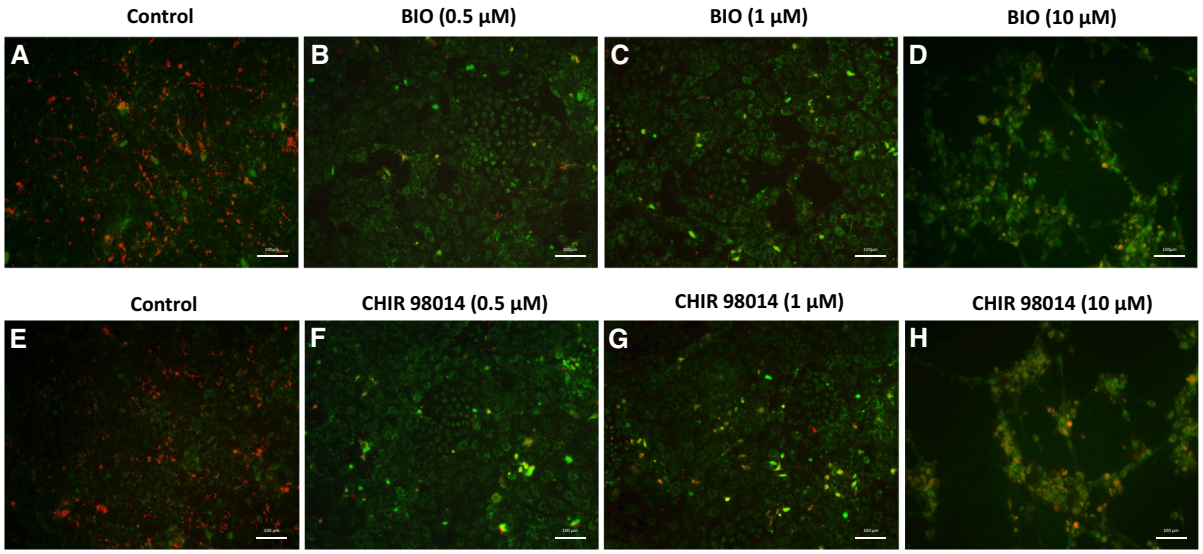

Fig. 3 Mitochondrial membrane potential ($\Delta\psi_m$) detection in 0.5, 1, and 10 µM of BIO (**a–d**) CHIR 98014 (**e–h**) treated H1975 cells by JC-1 staining. Untreated controls exhibited an increase in red fluorescence. 10 µM of BIO and CHIR 98014 exhibited green fluorescence with elongated phenotypic changes. Images were taken at × 10 magnification. All experiments were done in triplicates

BIO and CHIR 98014 reduces the migratory potential of H1975 cells

Cell migration is an important feature of aggressive tumors. The assay was performed to assess the trans-endothelial migratory potential of cancer cells in response to treatments with BIO and CHIR 98014 (Fig. 5). The H1975 cells were plated onto HUVEC-coated cell culture inserts of a trans-well system and treated with 0.5, 1, 10 µM of BIO and CHIR 98014 for 72 h. Control H1975 cells exhibited significant viability of migratory cells at 95.2% ± 5.3 (Fig. 5a). However, treatment with 0.5, 1 µM of BIO, and CHIR 98014 (Fig. 5b, f) exhibited a reduction in migrated cells, indicating the ability of GSK-3 inhibitors in reducing the migratory potential of H1975 cells. Reduction in migrated cells with 8.2% ± 2.5 (**$P < 0.01$) cell viability was observed in with 10 µM of BIO and 10.4% ± 1.9 (**$P < 0.01$) CHIR 98014 (Fig. 5i) treated cells compared to untreated controls.

Effects of BIO and CHIR 98014 on tumorsphere formation and Caspase-3/7 activation in H1975 cells

The tumorsphere formation was assessed following BIO and CHIR 98014 (0.5, 1, and 10 µM) treatments of H1975 cells cultured in a serum-free RPMI medium for 72 h (Shaheen et al. 2016). Control tumorspheres exhibited a size range of 98–123 µm before drug treatments (Fig. 6). On the other hand, treatments with 1 µM of BIO exhibited 79–88 µm tumorspheres, while CHIR 98014 (1 µM) treated cells resulted in 74–85 µm tumorspheres (Fig. 6c, g, i). However, following 10 µM treatments the tumorsphere sizes were significantly reduced to 41–47 µm (**$P < 0.01$) and 30–38 µm (**$P < 0.01$) respectively for BIO and CHIR (Fig. 6d, h, i). In the tumorspheres, the cleavage of caspase-3/7 was also observed following treatments with BIO and CHIR 98014 for 72 h (Fig. 7). Interestingly, significant cleavage of caspase-3/7 and immature formation of tumorspheres were observed in 10 µM BIO and CHIR 98014 treated cells (Fig. 7d, h). BIO (10 µM) exhibited 64.0% ± 6.6 increase in fluorescence intensity while CHIR 98014 (10 µM) exhibited 87.5% ± 1.9 increase in fluorescence intensity compared to untreated controls (Fig. 7i). At lower concentrations of BIO (0.5 and 1.0 µM) and CHIR

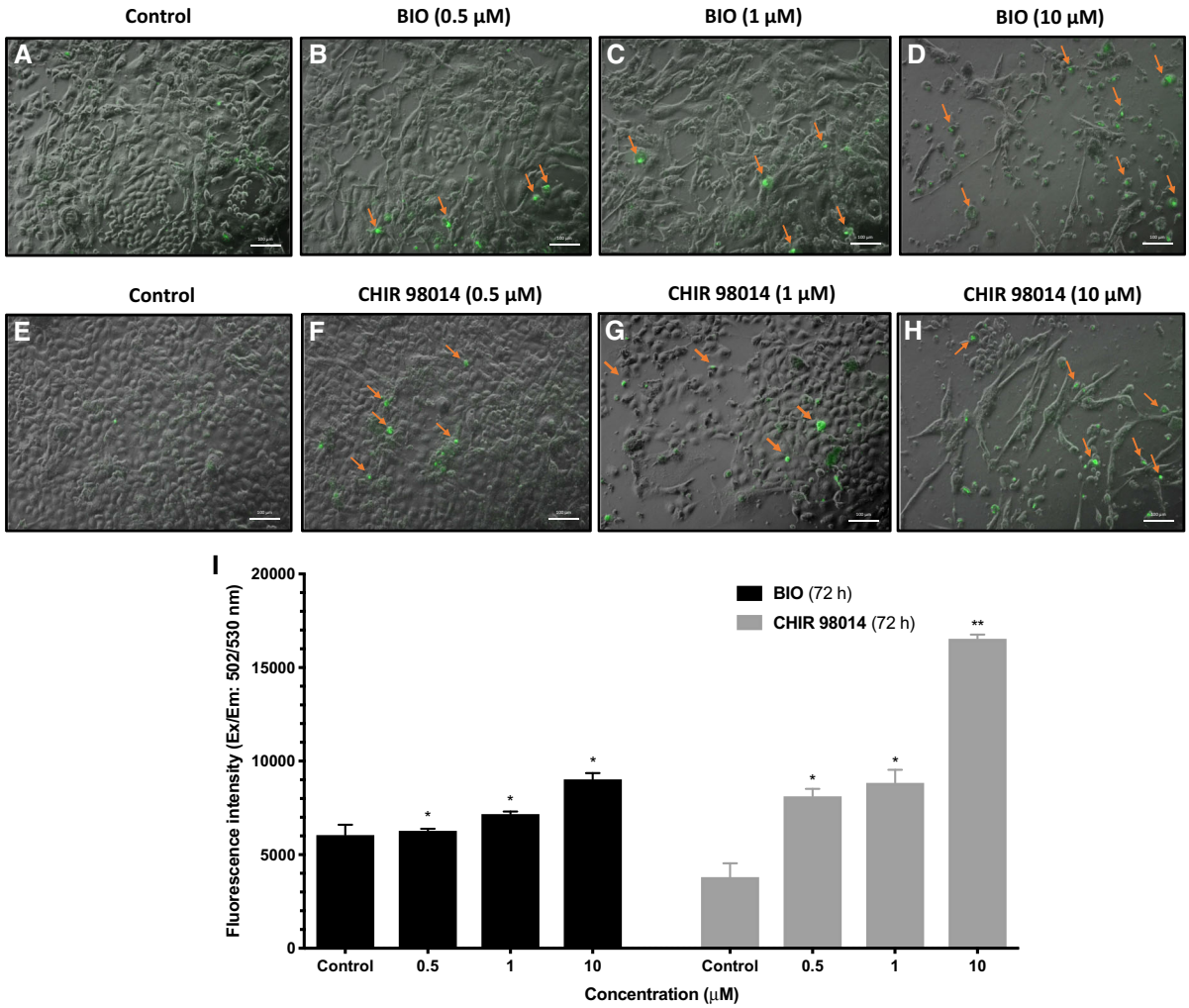

Fig. 4 Caspase-3/7 detection of 0.5, 1, and 10 µM of BIO (**a–d**) CHIR 98014 (**e–h**) treated H1975 cells by caspase-3/7 molecular probe. **i** Spectrofluorimetric quantification of 10 µM BIO and CHIR 98014 for 72 h exhibited caspase-3/7 cleavage evidenced by green fluorescence due to DEVD peptide cleavage. Images were taken at × 10 magnification. All experiments were done in triplicates

98014 (0.5 and 1.0 µM) increased caspase activation was evident along with the impact on the formation of tumorspheres. For example, 1 µM of BIO (Fig. 7c) exhibited 31.7% ± 2.7 increase in fluorescence intensity while 1 µM of CHIR 98014 (Fig. 7g) exhibited 86.3% ± 10.6 increase in fluorescence intensity compared to untreated controls. Treatment with 0.5 µM of CHIR 98014 showed changes that were non-significant.

BIO and CHIR 98014 reduces colony formation of H1975 cells

Colony formation is a key factor in assessing tumorigenesis. CFU assay was performed on 0.5, 1, and 10 µM BIO and CHIR 98014 treated H1975 cells (Fig. 8). Significant reduction in the formation of colonies were observed in both 10 µM BIO (82 colonies ± 16) (**$P < 0.01$) and CHIR 98014 (85 colonies ± 14) (**$P < 0.01$) at 72 h (Fig. 8a, b) compared to untreated controls (240 colonies ± 23). However, no significant changes were observed in 0.5 and 1 µM of BIO (Fig. 8a, c) and CHIR 98014

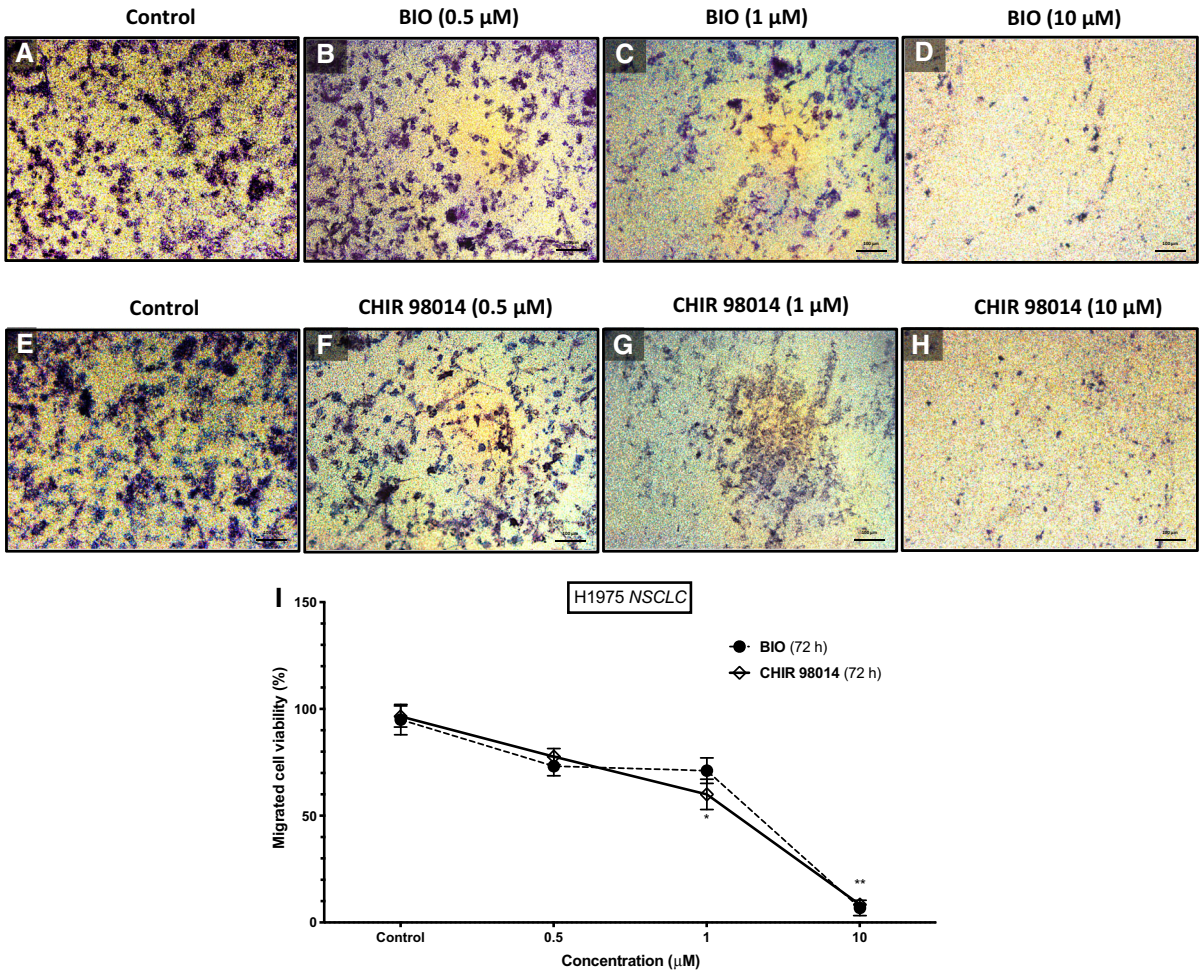

Fig. 5 Trans-endothelial migratory assay of 0.5, 1, and 10 µM of BIO (**a–d**) CHIR 98014 (**e–h**) treated H1975 cells. Untreated H1975 cells reported the highest potential for migration. **i** 10 µM of BIO and CHIR 98014 treatment exhibited 8.2% ± 2.5 (**P < 0.01) and 10.41% ± 1.9 (**P < 0.01), respectively. Images were taken at × 10 magnification. All experiments were done in triplicates

(Fig. 8b, c), treated cells, implying the ability of CHIR and BIO to reduce colony formation at higher concentrations.

BIO and CHIR 98014 phosphorylates GSK-3 (Ser9) and P53 in H1975 cells

GSK-3 is a serine-threonine kinase, which is responsible for multiple cellular processes were studied to identify the effect of BIO and CHIR 98014 on H1975 cells (Fig. 9). GSK-3 inhibitors are known to inhibit GSK-3 activity through activation of protein phosphorylation and thereby regulating the *wnt* pathway (Zhang et al. 2003). BIO and CHIR 98014 (Fig. 9a, b) were evidenced to significantly increase the phosphorylation of GSK-3 (Ser9) in a concentration-dependent manner. No significant changes were observed in total GSK-3 of all treated groups. Phosphorylation of P53 at the Ser15 position is reported to be critical for the transactivation of P53 (Loughery et al. 2014). An increase in phosphorylation of P53 was exhibited when cells were treated with 10 µM of BIO and CHIR 98014 (Fig. 9b, e). The levels of P21, which is a cyclin-dependent kinase (CDK) inhibitor and regulator of cell cycle progression were also investigated to observe the regulatory potential of BIO and CHIR 98014 through P21 activation (Abbas and Dutta 2009). Interestingly, a threefold increase (**P < 0.01) in P21

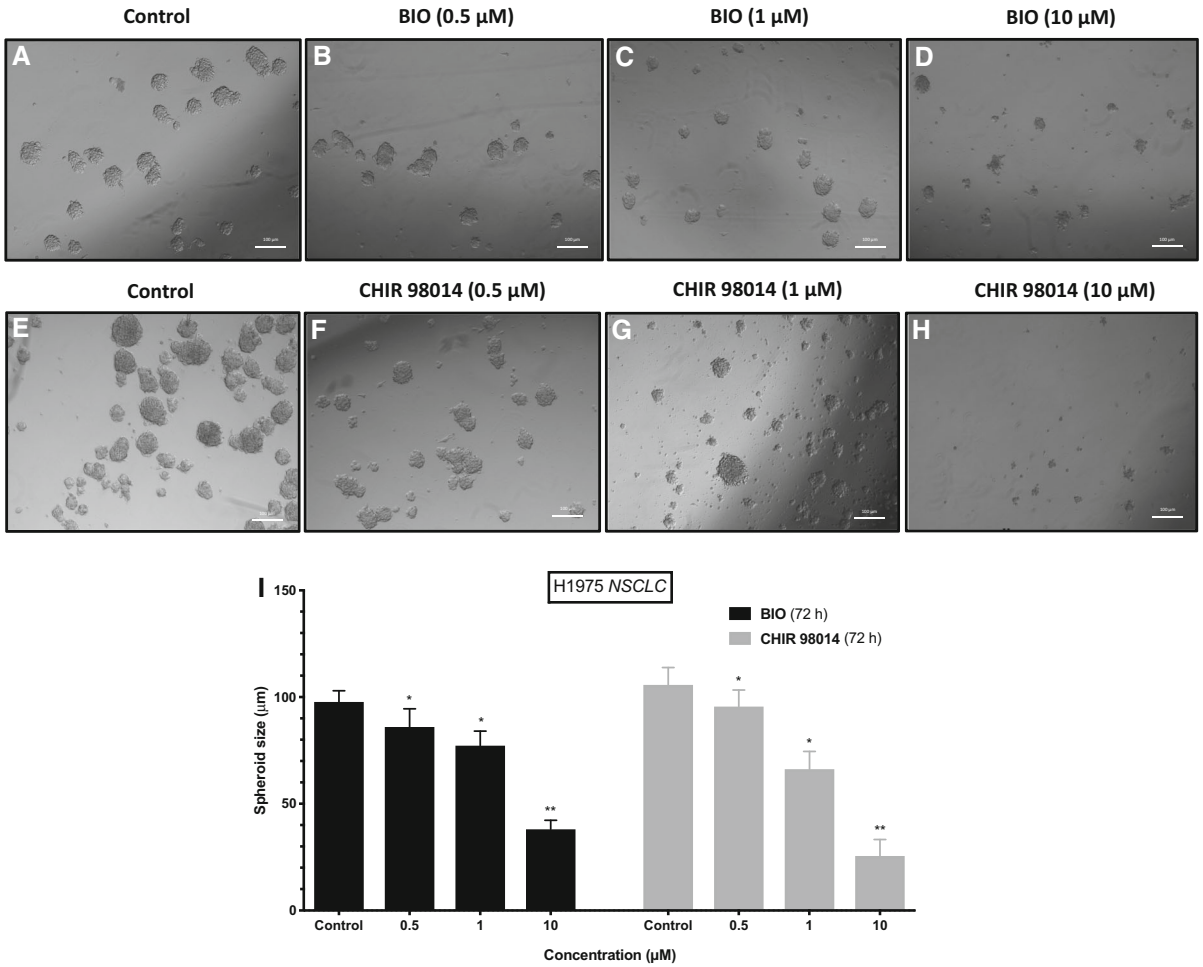

Fig. 6 Tumorsphere formation of 0.5, 1, and 10 µM of BIO (**a–d**) CHIR 98014 (**e–h**) treated H1975 cells. Untreated tumorsphere formation reported a size of (98–123 µM). **i** 10 µM of BIO and CHIR 98014 exhibited (41–47 µM) (**P < 0.01), and (41–47 µM) (**P < 0.01) tumorsphere sizes, respectively. Images were taken at × 10 magnification. All experiments were done in triplicates

was level was observed in 1 and 10 µM of CHIR 98014-treated cells (Fig. 9e). However, a 6.7-fold increase (**P < 0.01) in P21 expression was observed in BIO-treated cells with concentrations of 1 and 10 µM (Fig. 9b). Taken together, these results indicate an active involvement of P53 and P21 in BIO and CHIR 98014-mediated cell death.

BIO and CHIR 98014 downregulates XIAP while upregulating BAX and LC3B in H1975 cells

XIAP (X-linked inhibitor of apoptosis) is an inhibitor of caspases, which can lead to a significant increase in the cancer cell invasion (Chaudhary et al. 2016). The level of XIAP was studied to explore the effects of BIO and CHIR 98014 treatments on H1975 cells (Fig. 9a). XIAP exhibited no significant change in control, 0.5, 1 µM of BIO, and CHIR 98014-treated H1975 cells, but the levels were significantly decreased with 10 µM of BIO and CHIR 98014 treatments (Fig. 9c, f). BAX, a nuclear-encoded protein responsible for mitochondrial membrane damage, also showed significant upregulation of 1.96-fold change (**P < 0.01) with 10 µM of BIO and 2.3-fold change (**P < 0.01) with 10 µM of CHIR 98014 treatments (Fig. 9c, f). The results obtained with BAX, in addition to the changes in the MMP, demonstrates the ability of BIO and CHIR 98014 in inducing

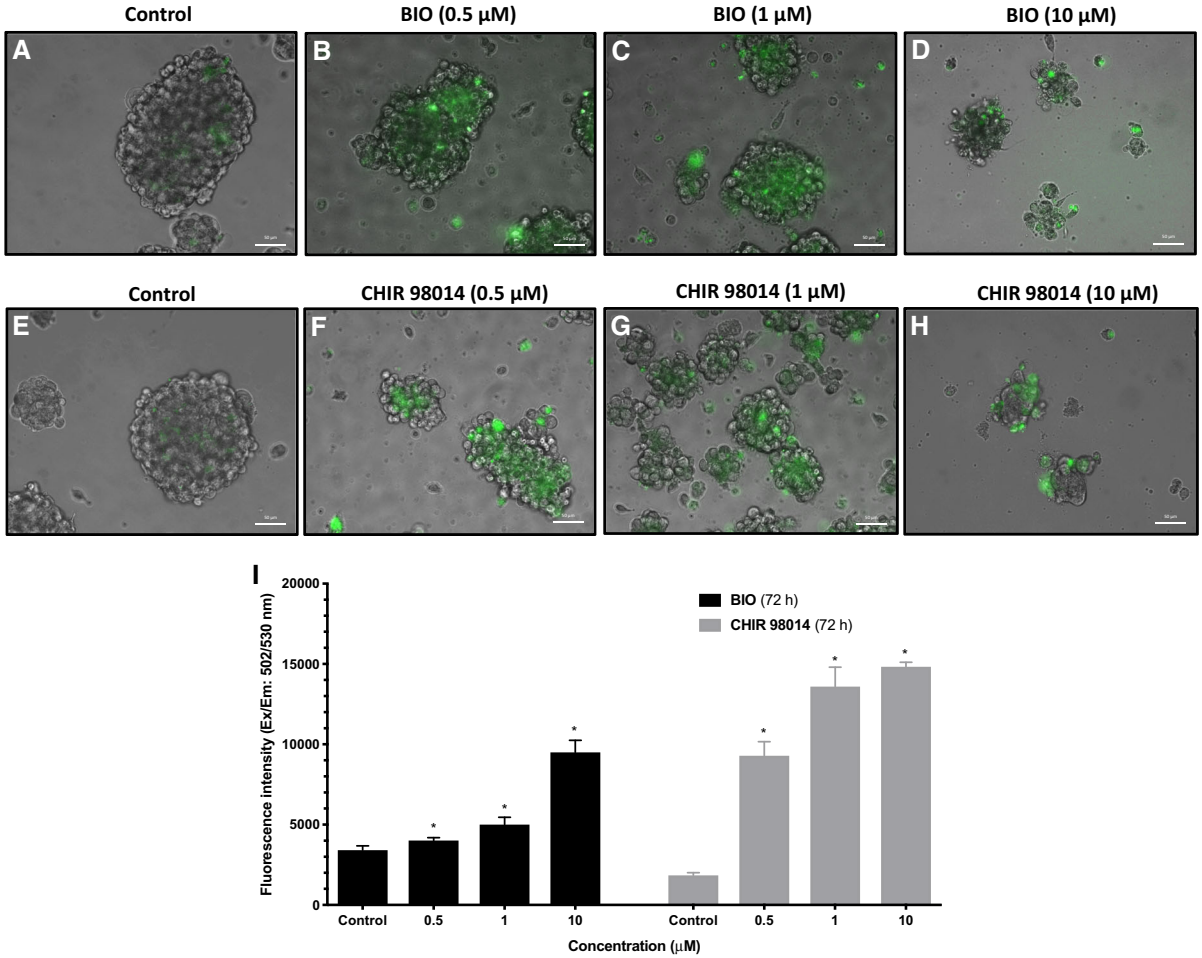

Fig. 7 Caspase-3/7 cleavage of 0.5, 1, and 10 µM of BIO (**a–d**) CHIR 98014 (**e–h**) treated H1975 tumorspheres. **i** 10 µM of BIO and CHIR 98014 exhibited a significant increase in green fluorescence indicative of caspase-3/7 cleavage due to DEVD cleavage. Images were taken at × 40 magnification. All experiments were done in triplicates

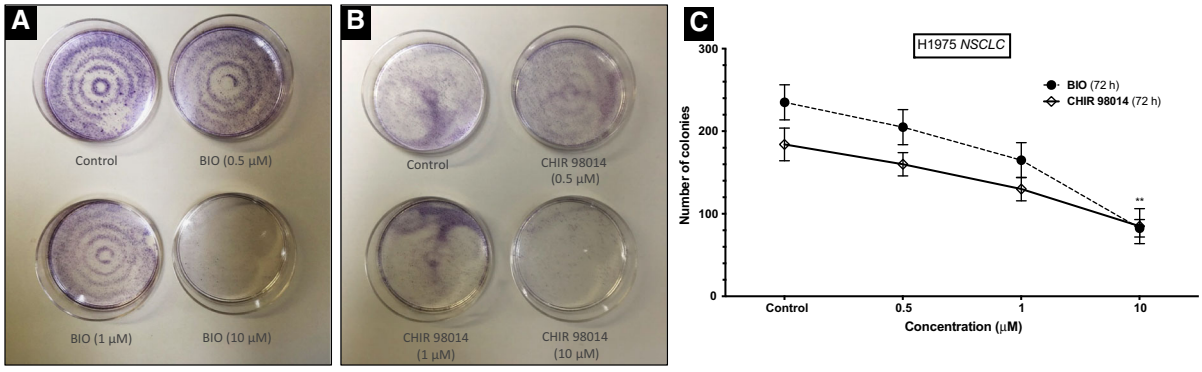

Fig. 8 Colony Formation unit assay of 0.5, 1, and 10 µM of BIO (**a**) CHIR 98014 (**b**) treated H1975 cells. Untreated H1975 cells reported the highest potential for colony formation. **c** Untreated H1975 cells exhibited (240 colonies ± 23) while 10 µM BIO and CHIR 98014 exhibited reduction in colony formation of (100 colonies ± 20) (**P < 0.01). All experiments were done in triplicates

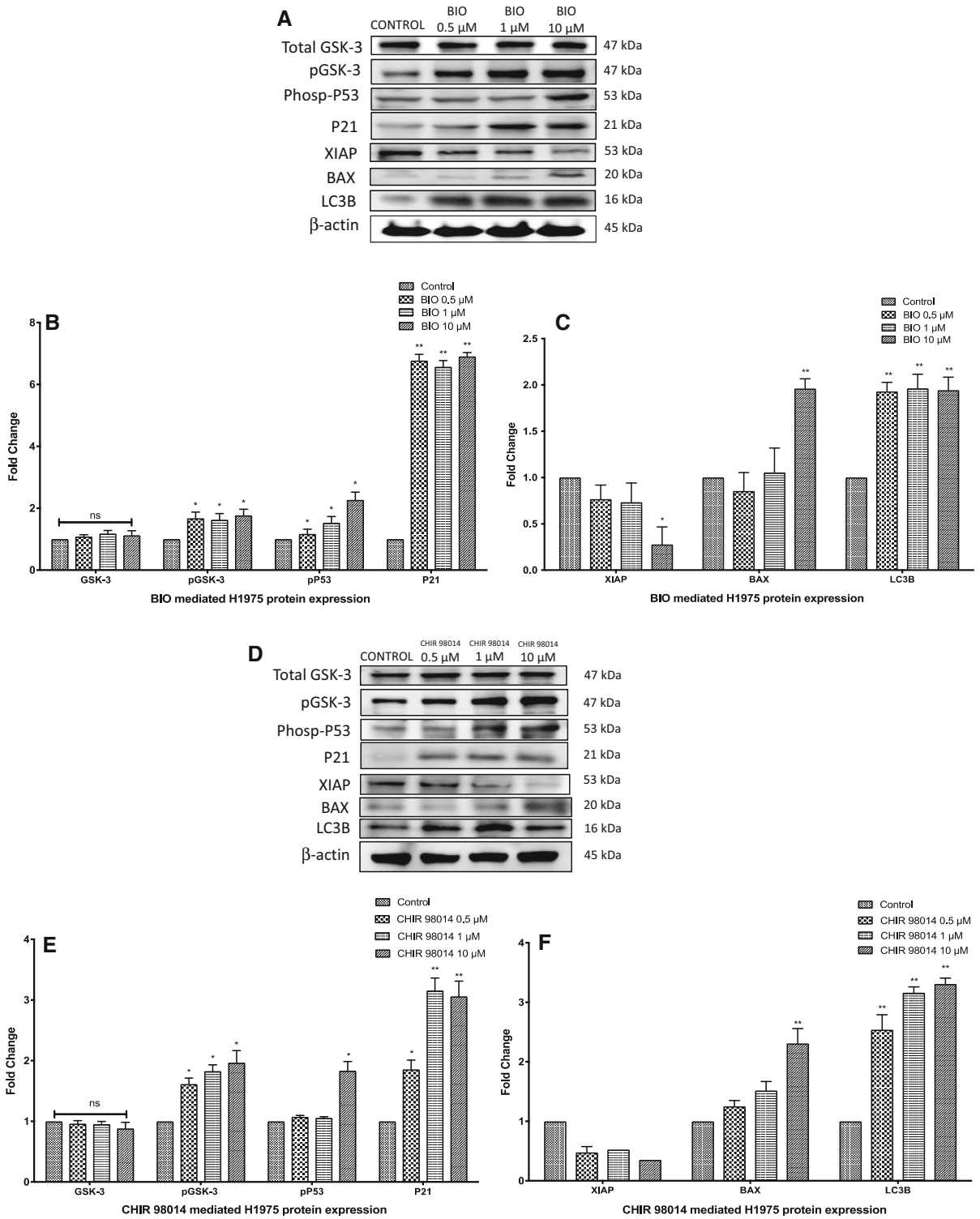
A
CONTROL
BIO 0.5 μM
BIO 1 μM
BIO 10 μM
Total GSK-3
pGSK-3
Phosp-P53
P21
XIAP
BAX
LC3B
β-actin
47 kDa
47 kDa
53 kDa
21 kDa
53 kDa
20 kDa
16 kDa
45 kDa
B
Control
BIO 0.5 μM
BIO 1 μM
BIO 10 μM
Fold Change
ns
GSK-3
pGSK-3
pP53
P21
BIO mediated H1975 protein expression
C
XIAP
BAX
LC3B
BIO mediated H1975 protein expression
D
CHIR 98014 0.5 μM
CHIR 98014 1 μM
CHIR 98014 10 μM
E
CHIR 98014 mediated H1975 protein expression
F

◀**Fig. 9** Protein expression studies of 0.5, 1, and 10 μM of BIO (**a–c**) CHIR 98014 (**d–f**) treated H1975 cells. BAX, showed a significant upregulation of 1.96-fold change (**P < 0.01) and 2.3-fold change (**P < 0.01) with 10 μM of BIO and CHIR 98014, respectively. The LC3B protein exhibited significant upregulation of 1.9-fold change (**P < 0.01) and 3.3-fold (**P < 0.01) with 10 μM of BIO and CHIR 98014, respectively, compared to untreated controls. All experiments were done in triplicates

mitochondrial membrane damage. A similar effect was reported after treating the cancer cells with GSK-3 inhibitors, which led to increased oxidative stress and mitochondrial dysfunction (Guidotti et al. 2017). LC3B, ubiquitin-like protein present at the autophagosomal membranes, was analyzed to identify the autophagic response following BIO and CHIR 98014 treatments. The LC3B protein exhibited a significant upregulation by 1.9-fold change (**P < 0.01) in BIO-treated H1975 cells at10 μM concentrations (Fig. 9c). On the other hand, H1975 cells treated with 10 μM of CHIR 98014 exhibited 3.3-fold (**P < 0.01) upregulation compared to untreated controls (Fig. 9f). These results indicate the ability of BIO and CHIR 98014 to induce autophagy while regulating apoptosis-related proteins.

BIO and CHIR 98014 induces the activation of caspases in H1975 cells

Membrane blebbing and cell shrinkage leading to apoptosis are mediated by effector caspase-9, which is also required for ROS (Zuo et al. 2009). Caspase-9, which is a regulator of intrinsic apoptosis, exhibited significant cleavage after treating the cells with 10 μM of BIO and CHIR 98014 (Fig. 10a, d). Though cleaved caspase-9 (37 kDa) was observed in 0.5, and 1 μM of BIO and CHIR 98014 treated cells significant cleavage of caspase-9 (35 kDa) was observed following 10 μM of CHIR 98014 treatments (Fig. 10c, f). Caspase-3 is responsible for normal development and cell death, leading to apoptotic chromatin condensation and DNA fragmentation (Porter and Jänicke 1999). Total caspase-3 (47 kDa) exhibited a 1.5-fold increase with 10 μM of BIO (**P < 0.01) (Fig. 10b) and 2.4-fold (**P < 0.01) increase with 10 μM of CHIR 98014 treated cells (Fig. 10e). These results together suggest the ability of BIO and CHIR 98014 to activate caspases 9 and 3, leading to apoptosis.

Discussion

GSK-3 inhibitors are emerging tools for clinical interventions in cancer and represent a niche area in combinational and differentiation therapy (Mathuram et al. 2018). Previous studies on BIO, a highly selective GSK-3 inhibitor has been reported to reduce cell viability in neuroblastoma cells (Duffy et al. 2014), and also inhibit epithelial-mesenchymal transition in triple-negative breast cancer cells (Vijay et al. 2019), while enhancing TRAIL-mediated apoptosis in human gastric adenocarcinoma cells (Wu et al. 2018). Interestingly, BIO has been reported to be protective to normal cells by activating antioxidant responses against DNA damage inducing agents (Sklirou et al. 2017). CHIR 98014, a highly selective GSK-3 inhibitor, has been reported to reduce oxygen–glucose deprivation (OGD) and simulated reperfusion-induced cell injury in human neuron-like cells (Lin et al. 2011). CHIR 98014 was also reported to enhance insulin-stimulated glucose transport in both in vitro and in vivo systems (Ring et al. 2003). Based on these previous reports, our investigations elucidate the possible mechanism of cell death as a consequence of GSK-3 inhibition using BIO and CHIR 98014. Incidentally, BIO and CHIR 98014 generated ROS, leading to subsequent mitochondrial distress, demonstrating their role in organelle damage. Our results also demonstrate significant cell death following treatment with BIO and CHIR 98014 in a concentration-dependent manner. On the contrary, the proliferation of lung cancer cells has been reported to be correlated with the overexpression of GSK-3β, and experimental evidence has shown that GSK-3 inhibition leads to a reduction of cell survival (Xie and Wang 2017; Zeng et al. 2014). In our study, notable cell death was observed even at lower concentrations in both BIO and CHIR 98014-treated H1975 cells after 72 h. However, no significant cell death was observed in H460 cells after 24, 48, and 72 h of treatments with lower concentrations of BIO and CHIR 98014. This could be attributed to the KRAS mutations found in H460 cells, which might be conferring drug resistance (Pao et al. 2005). Additionally, a significant increase in the anti-proliferative activity of BIO and CHIR 98014 was observed in H1975 cells, which could be due to the upregulation of P21 (Chen et al. 2015). Our observations confirmed the generation of ROS as one of the major contributors for BIO and CHIR 98014-mediated

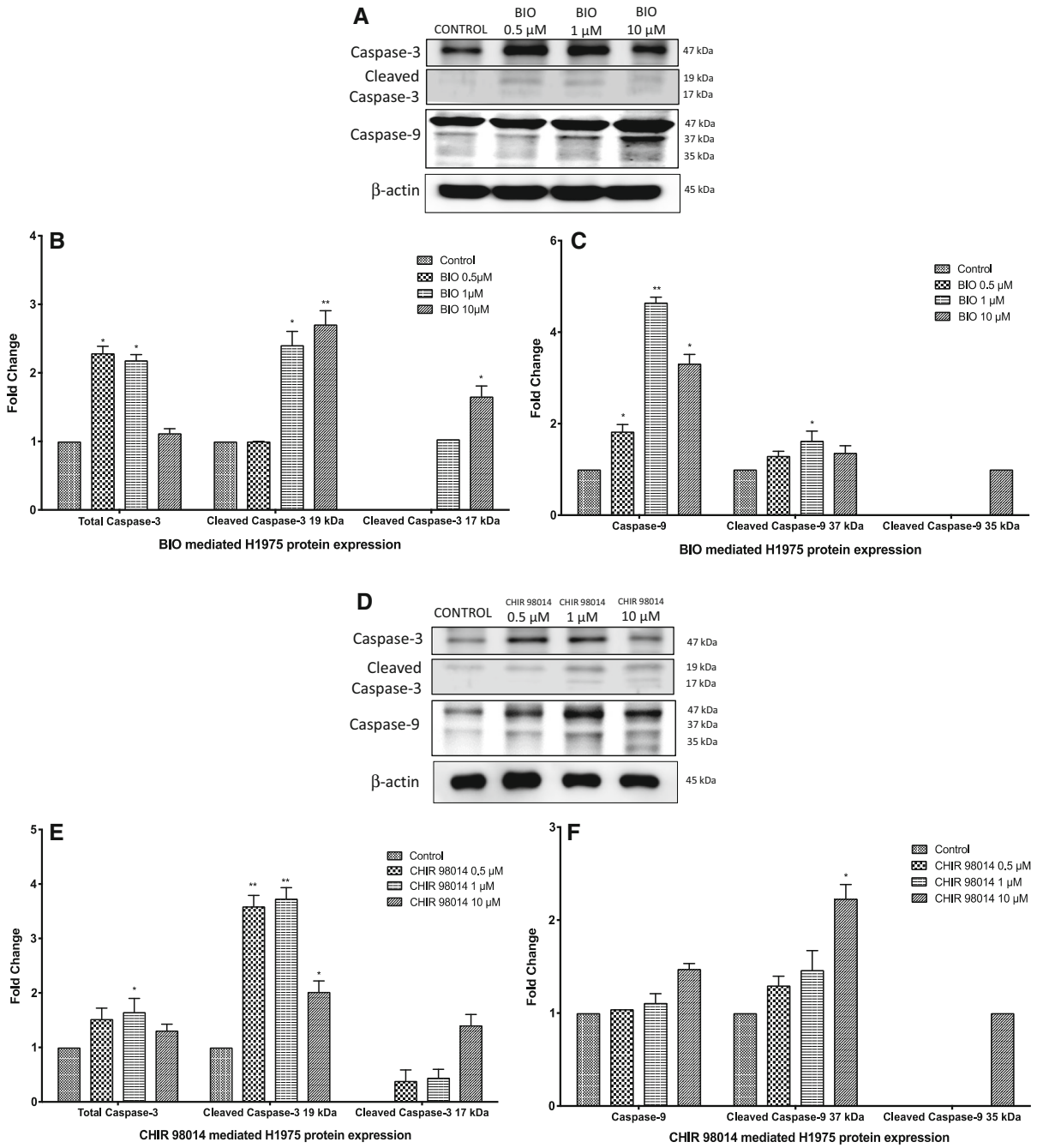

Fig. 10 Protein analysis of 0.5, 1, and 10 µM of BIO (**a–c**) CHIR 98014 (**d–f**) treated H1975 cells. 10 µM of BIO and CHIR 98014 exhibited upregulation of cleaved caspase-3 (19 kDa) at 1.5-fold (**P < 0.01) and 2.4-fold (**P < 0.01), respectively. All experiments were done in triplicates

cell death. Our results also confirm that mitochondrial membrane potential (Δψm) damage in BIO and CHIR 98014-treated cells, where depolarization leading to JC-1 monomer accumulation was observed in both treatments while high mitochondrial membrane potential due to accumulation of JC-1 polymer was observed in untreated control cells. The dysregulation of mitochondrial membrane function could be due to

the ability of BIO and CHIR 98014 to alter the oxidative metabolism of the mitochondria leading to cell death processes such as autophagy or apoptosis (Van Houten et al. 2016). Several genetic regulators of mitochondrial membrane depolarization, such as Cck (cholecystokinin), Alox12, (arachidonate 12-lipoxygenase), Dcn (decorin) can play important roles in the fate of cells undergoing oxidative stress (Chirichigno et al. 2002). The cellular levels of ROS and the consequent alterations of MMP have clinical relevance because of their ability to induce DNA strand breakage in cancer cells but not in normal cells (Marrocco et al. 2017). Additionally, cleavage of caspase-3/7 following BIO and CHIR 98014 treatments confirm the involvement of caspases in inducing cell death of H1975 cells. The activation of caspase-3 appears to be due to the generation of ROS, which in turn leads to mitochondrial damages in H1975 cells (Chen et al. 1998). ROS, an inevitable byproduct of redox reaction has been reported to activate the transcription factor NF-κB (nuclear factor kappa-light-chain-enhancer of activated B cells) through regulation of MAP kinase cascades (Perkins 2000). Interestingly, increased oxidative stress could also inactivate transcription factor AP-1 (activator protein-1) through reversible oxidation of their SH-group (Morel and Barouki 1999). Thus, it is evident that accumulation of ROS due to elevated oxidative stress could play an important role in the genetic regulation of cancer cell death (Yang et al. 2018). In addition, the reduction in the invasive and migratory potential of H1975 cells suggests that the GSK-3 inhibitors can be good drug candidates for preventing metastasis (van Zijl et al. 2011). To further substantiate these findings, our results show that BIO and CHIR 98014 can reduce the formation of tumorspheres, which is another indicator of anti-metastatic ability (Klameth et al. 2017). The reduction in the formation of tumorspheres was evidently accompanied by caspase 3/7 cleavage in BIO and CHIR 98014-treated tumorspheres, which further portrays the ability of GSK-3 inhibition impacting diverse mechanisms leading to cell cycle arrest and cell death. Our results are the first-time evidence that confirms the reduction in tumorsphere formation when H1975 cells are treated with BIO and CHIR 98014. Interestingly, a loose aggregation of cells was also observed following BIO and CHIR 98014 treatments, while clearly defined aggregation of cells was observed in non-treated cells. Altogether, these results indicate that inhibition of cell adhesion could lead to a decrease in cancer cell survival due to increased exposure to the anticancer drug effects. Our CFU experiments also showed a significant reduction in the formation of colonies after BIO and CHIR 98014 treatments indicating the ability of GSK-3 inhibitors to reduce colony forming ability of cancer cells. Furthermore, increased phosphorylation of GSK-3 (Ser9) that was observed in western blotting analysis suggests that phosphorylation-mediated inhibition of GSK-3 activity by BIO and CHIR 98014 treatments (Zhang et al. 2003). In addition to the changes in GSK-3, the phosphorylation of P53 was also increased following BIO and CHIR 98014 treatments, which is suspected to be due to ROS generation and mitochondrial dysfunction leading to activation of target specific kinases (Yogosawa and Yoshida 2018). The phosphorylation of P53 has also been reported to induce cell cycle arrest (Chen et al. 2015), which is evidenced in our studies when treatments with BIO and CHIR 98014 exerted significant upregulation of P21, a well-known mediator of CDK inhibition and cell cycle arrest (Lee et al. 2007). Furthermore, XIAP was downregulated in a concentration-dependent manner following GSK-3 inhibition, suggesting a caspase-mediated cell death (Suzuki et al. 2001). Upregulation of BAX, along with the activation of caspases 3 and 9, confirms their participation in executing apoptosis following treatment of H1975 cells with GSK-3 inhibitors. Intriguingly, LC3B, a known marker of autophagy, was also significantly elevated when the H1975 cells were treated with BIO and CHIR 98014 suggesting a possible involvement of autophagic response also as a result of pharmacological inhibition of GSK-3 (Parr et al. 2016). Similar regulation of both apoptotic and autophagic cell fate were observed when GSK-3 was inhibited with MG132 in human breast epithelial cell (Choi et al. 2012). Taking together these findings, our results provide strong evidence that GSK-3 inhibitors can induce cell death through both autophagy as well as apoptotic mechanisms.

Conclusion

The biological relevance of GSK-3 is increasingly evident, and recent studies are exposing the growing

roles of this enigmatic kinase. Our study concludes by stressing the importance of GSK-3 as an important drug-target for initiating pharmacological interventions, with emphasis on CHIR 98014 as a more potent inhibitor compared to BIO in inducing apoptotic cell death in H1975 cells. Further research is needed to establish the differences of mechanisms exerted by BIO and CHIR 98014 in other cancer cells.

Compliance with ethical standards

Conflict of interest The author declares no conflict of interest.

References

Abbas T, Dutta A (2009) p21 in cancer: intricate networks and multiple activities. Nat Rev Cancer 9:400–414. https://doi.org/10.1038/nrc2657

Adderley H, Blackhall FH, Lindsay CR (2019) KRAS-mutant non-small cell lung cancer: converging small molecules and immune checkpoint inhibition. EBioMedicine 41:711–716. https://doi.org/10.1016/j.ebiom.2019.02.049

Anraku T et al (2020) Clinically relevant GSK-3β inhibitor 9-ING-41 is active as a single agent and in combination with other antitumor therapies in human renal cancer. Int J Mol Med 45:315–323. https://doi.org/10.3892/ijmm.2019.4427

Arefi SMA, Daria T, Claude V, James JF (2020) A biomechanical model for the transendothelial migration of cancer cells. Phys Biol 17(3):036004

Cao Y et al (2017) The use of human umbilical vein endothelial cells (HUVECs) as an in vitro model to assess the toxicity of nanoparticles to endothelium: a review. J Appl Toxicol 37:1359–1369. https://doi.org/10.1002/jat.3470

Chaudhary AK, Yadav N, Bhat TA, O'Malley J, Kumar S, Chandra D (2016) A potential role of X-linked inhibitor of apoptosis protein in mitochondrial membrane permeabilization and its implication in cancer therapy. Drug Discov Today 21:38–47. https://doi.org/10.1016/j.drudis.2015.07.014

Chen Y-C, Lin-Shiau S-Y, Lin J-K (1998) Involvement of reactive oxygen species and caspase 3 activation in arsenite-induced apoptosis. J Cell Physiol 177:324–333

Chen A et al (2015) The role of p21 in apoptosis proliferation, cell cycle arrest, and antioxidant activity in UVB-irradiated human HaCaT keratinocytes. Med Sci Monit Basic Res 21:86–95. https://doi.org/10.12659/MSMBR.893608

Chirichigno JW, Manfredi G, Beal MF, Albers DS (2002) Stress-induced mitochondrial depolarization and oxidative damage in PSP cybrids. Brain Res 951:31–35. https://doi.org/10.1016/S0006-8993(02)03101-3

Choi C-H, Lee B-H, Ahn S-G, Oh S-H (2012) Proteasome inhibition-induced p38 MAPK/ERK signaling regulates autophagy and apoptosis through the dual phosphorylation of glycogen synthase kinase 3β. Biochem Biophys Res Commun 418:759–764. https://doi.org/10.1016/j.bbrc.2012.01.095

Duffy DJ, Krstic A, Schwarzl T, Higgins DG, Kolch W (2014) GSK3 inhibitors regulate MYCN mRNA levels and reduce neuroblastoma cell viability through multiple mechanisms, including p53 and wnt signaling. Mol Cancer Ther 13:454–467. https://doi.org/10.1158/1535-7163.Mct-13-0560-t

Genovese S, Epifano F, Preziuso F, Slater J, Nangia-Makker P, Majumdar APN, Fiorito S (2020) Gercumin synergizes the action of 5-fluorouracil and oxaliplatin against chemoresistant human cancer colon cells. Biochem Biophys Res Commun 522:95–99. https://doi.org/10.1016/j.bbrc.2019.11.068

Guidotti S et al (2017) Glycogen synthase kinase-3β inhibition links mitochondrial dysfunction extracellular matrix remodelling and terminal differentiation in chondrocytes. Sci Rep 7:12059. https://doi.org/10.1038/s41598-017-12129-5

Kalyanaraman B et al (2012) Measuring reactive oxygen and nitrogen species with fluorescent probes: challenges and limitations. Free Rad Biol Med 52:1–6. https://doi.org/10.1016/j.freeradbiomed.2011.09.030

Kazi A et al (2018) GSK3 suppression upregulates β-catenin and c-Myc to abrogate KRas-dependent tumors. Nat Commun 9:5154. https://doi.org/10.1038/s41467-018-07644-6

Klameth L et al (2017) Small cell lung cancer: model of circulating tumor cell tumorospheres in chemoresistance. Sci Rep 7:5337–5337. https://doi.org/10.1038/s41598-017-05562-z

Lee JY, Yu SJ, Park YG, Kim J, Sohn J (2007) Glycogen synthase kinase 3beta phosphorylates p21WAF1/CIP1 for proteasomal degradation after UV irradiation. Mol Cell Biol 27:3187–3198. https://doi.org/10.1128/MCB.01461-06

Lin D, Li G, Zuo Z (2011) Volatile anesthetic post-treatment induces protection via inhibition of glycogen synthase kinase 3β in human neuron-like cells. Neuroscience 179:73–79. https://doi.org/10.1016/j.neuroscience.2011.01.055

Loughery J, Cox M, Smith LM, Meek DW (2014) Critical role for p53-serine 15 phosphorylation in stimulating transactivation at p53-responsive promoters. Nucleic Acids Res 42(12):7666–7680. https://doi.org/10.1093/nar/gku501

Marrocco I, Altieri F, Peluso I (2017) Measurement and clinical significance of biomarkers of oxidative stress in humans. Oxid Med Cell Longev. https://doi.org/10.1155/2017/6501046

Mathuram TL, Ravikumar V, Reece LM, Sasikumar CS, Cherian KM (2017) Correlative studies unravelling the possible mechanism of cell death in tideglusib-treated human ovarian teratocarcinoma-derived PA-1. Cells 36:321–344. https://doi.org/10.1615/JEnvironPatholToxicolOncol.2017025018

Mathuram TL, Reece LM, Cherian KM (2018) GSK-3 Inhibitors: a double-edged sword? An update on tideglusib. Drug Res (Stuttg) 68:436–443. https://doi.org/10.1055/s-0044-100186

Morel Y, Barouki R (1999) Repression of gene expression by oxidative stress. Biochem J 342(Pt 3):481–496

Muller WA, Luscinskas FW (2008) Assays of transendothelial migration in vitro. Methods Enzymol 443:155–176. https://doi.org/10.1016/S0076-6879(08)02009-0

Pao W et al (2005) KRAS mutations and primary resistance of lung adenocarcinomas to gefitinib or erlotinib. PLoS Med 2:e17–e17. https://doi.org/10.1371/journal.pmed.0020017

Parr C, Carzaniga R, Gentleman SM, Van Leuven F, Walter J, Sastre M (2016) Correction for parr et al., glycogen synthase kinase 3 inhibition promotes lysosomal biogenesis and autophagic degradation of the amyloid-β precursor protein. Mol Cell Biol 36:1219–1219. https://doi.org/10.1128/MCB.00086-16

Perelman A, Wachtel C, Cohen M, Haupt S, Shapiro H, Tzur A (2012) JC-1: alternative excitation wavelengths facilitate mitochondrial membrane potential cytometry. Cell Death Dis 3:e430–e430. https://doi.org/10.1038/cddis.2012.171

Perkins ND (2000) The Rel/NF-κB family: friend and foe. Trends Biochem Sci 25:434–440. https://doi.org/10.1016/S0968-0004(00)01617-0

Porter AG, Jänicke RU (1999) Emerging roles of caspase-3 in apoptosis. Cell Death Diff 6:99–104. https://doi.org/10.1038/sj.cdd.4400476

Ring DB et al (2003) Selective glycogen synthase kinase 3 inhibitors potentiate insulin activation of glucose transport and utilization in vitro and in vivo. Diabetes 52:588–595. https://doi.org/10.2337/diabetes.52.3.588

Rudd CE, Chanthong K, Taylor A (2020) Small molecule inhibition of GSK-3 specifically inhibits the transcription of inhibitory co-receptor LAG-3 for enhanced anti-tumor immunity. Cell Rep 30:2075–2082.e2074. https://doi.org/10.1016/j.celrep.2020.01.076

Shaheen S, Ahmed M, Lorenzi F, Nateri AS (2016) Spheroid-formation (Colonosphere) assay for in vitro assessment and expansion of stem cells in colon cancer. Stem Cell Rev Rep 12:492–499. https://doi.org/10.1007/s12015-016-9664-6

Siegel RL, Miller KD, Jemal A (2020) Cancer statistics, 2020. CA Cancer J Clin 70:7–30. https://doi.org/10.3322/caac.21590

Sklirou AD, Gaboriaud-Kolar N, Papassideri I, Skaltsounis A-L, Trougakos IP (2017) 6-bromo-indirubin-3′-oxime (6BIO), a Glycogen synthase kinase-3β inhibitor, activates cytoprotective cellular modules and suppresses cellular senescence-mediated biomolecular damage in human fibroblasts. Sci Rep 7:11713. https://doi.org/10.1038/s41598-017-11662-7

Suzuki Y, Nakabayashi Y, Nakata K, Reed JC, Takahashi R (2001) X-linked inhibitor of apoptosis protein (XIAP) inhibits caspase-3 and -7 in distinct modes. J Biol Chem 276:27058–27063. https://doi.org/10.1074/jbc.M102415200

Van Houten B, Hunter SE, Meyer JN (2016) Mitochondrial DNA damage induced autophagy, cell death, and disease. Front Biosci 21:42–54. https://doi.org/10.2741/4375

van Zijl F, Krupitza G, Mikulits W (2011) Initial steps of metastasis: cell invasion and endothelial transmigration. Mutat Res 728:23–34. https://doi.org/10.1016/j.mrrev.2011.05.002

Vijay GV et al (2019) GSK3β regulates epithelial-mesenchymal transition and cancer stem cell properties in triple-negative breast cancer. Breast Cancer Res 21:37. https://doi.org/10.1186/s13058-019-1125-0

Walz A et al (2017) Molecular pathways: revisiting glycogen synthase kinase-3β as a target for the treatment of cancer clinical. Cancer Res 23:1891–1897. https://doi.org/10.1158/1078-0432.Ccr-15-2240

Wojtowicz JM, Kee N (2006) BrdU assay for neurogenesis in rodents. Nat Protoc 1:1399–1405. https://doi.org/10.1038/nprot.2006.224

Wu Y-Y, Hsieh C-T, Chiu Y-M, Chou S-C, Kao J-T, Shieh D-C, Lee Y-J (2018) GSK-3 inhibitors enhance TRAIL-mediated apoptosis in human gastric adenocarcinoma cells. PLoS ONE 13:e0208094. https://doi.org/10.1371/journal.pone.0208094

Xie S, Wang C (2017) GSK-3 inhibition suppresses lung cancer cell survival, metastasis and proliferation through down-regulation the phosphorylation sites of CAP1. Eur Resp J 50:PA4204. https://doi.org/10.1183/1393003.congress-2017.PA4204

Yang H, Villani RM, Wang H, Simpson MJ, Roberts MS, Tang M, Liang X (2018) The role of cellular reactive oxygen species in cancer chemotherapy. J Exp Clin Cancer Res 37:266. https://doi.org/10.1186/s13046-018-0909-x

Yogosawa S, Yoshida K (2018) Tumor suppressive role for kinases phosphorylating p53 in DNA damage-induced apoptosis. Cancer Sci 109:3376–3382. https://doi.org/10.1111/cas.13792

Yu A-S, Zhao L (2016) Effects of the GSK-3β inhibitor (2Z,3E)-6-bromoindirubin-3′-oxime upon ovarian cancer cells. Tumor Biol 37:4857–4864. https://doi.org/10.1007/s13277-015-4344-8

Zeng J et al (2014) GSK3β overexpression indicates poor prognosis and its inhibition reduces cell proliferation and survival of non-small cell lung cancer cells. PLoS ONE 9:e91231–e91231. https://doi.org/10.1371/journal.pone.0091231

Zhang F, Phiel CJ, Spece L, Gurvich N, Klein PS (2003) Inhibitory phosphorylation of glycogen synthase kinase-3 (GSK-3) in response to lithium: evidence for autoregulation of GSK-3. J Biol Chem 278:33067–33077. https://doi.org/10.1074/jbc.M212635200

Zuo Y, Xiang B, Yang J, Sun X, Wang Y, Cang H, Yi J (2009) Oxidative modification of caspase-9 facilitates its activation via disulfide-mediated interaction with Apaf-1. Cell Res 19:449–457. https://doi.org/10.1038/cr.2009.19